



CHORUS

This is the accepted manuscript made available via CHORUS. The article has been published as:

Fundamental Precision Bounds for Three-Dimensional Optical Localization Microscopy with Poisson Statistics

Mikael P. Backlund, Yoav Shechtman, and Ronald L. Walsworth

Phys. Rev. Lett. **121**, 023904 — Published 11 July 2018

DOI: [10.1103/PhysRevLett.121.023904](https://doi.org/10.1103/PhysRevLett.121.023904)

Fundamental precision bounds for three-dimensional optical localization microscopy with Poisson statistics

Mikael P. Backlund,^{1,2} Yoav Shechtman,³ and Ronald L. Walsworth^{1,2}

¹*Harvard-Smithsonian Center for Astrophysics, Cambridge, MA 02138, USA*

²*Department of Physics, Harvard University, Cambridge, MA 02138, USA*

³*Department of Biomedical Engineering, Technion, Israel Institute of Technology, Haifa, Israel*

(Dated: May 21, 2018)

Point source localization is a problem of persistent interest in optical imaging. In particular, a number of widely used biological microscopy techniques rely on precise three-dimensional localization of single fluorophores. As emitter depth localization is more challenging than lateral localization, considerable effort has been spent on engineering the response of the microscope in a way that reveals increased depth information. Here we prove the (sub)optimality of these approaches by deriving and comparing to the measurement-independent quantum Cramér-Rao bound (QCRB). We show that existing methods for depth localization with single-objective collection exceed the QCRB, and gain insight into the bound by proposing an interferometer arrangement that approaches it. We also show that for collection with two opposed objectives, an established interferometric technique globally reaches the QCRB in all three dimensions simultaneously, and so represents an interesting case study from the point of view of quantum multiparameter estimation.

Precise spatial localization of single fluorescent emitters is at the heart of a number of important advanced microscopy techniques, including defect-based sensing [1–4] and single-molecule-based tracking and super-resolution imaging [5–7]. For three-dimensional (3D) imaging, extracting the emitter’s depth (z position) is an enduring challenge. Microscopists have addressed this by engineering the microscope’s point spread function (PSF) in ways that improve the attainable depth precision [8–20], effectively reducing the associated Cramér-Rao bound (CRB) [21]. But what is the optimal depth precision that can be attained by any such microscope engineering approach? Are existing techniques optimal? In this work we address these fundamental questions by deriving the measurement-independent limit, the quantum Cramér-Rao bound (QCRB) [22], leading to important new insights for 3D optical localization microscopy.

Throughout this Letter we consider semiclassical photodetection in the limit of Poisson counting statistics [23–27]. This simplified approach ignores (anti)bunching, but is nonetheless relevant to many practical microscopy implementations and is ubiquitous in the fluorescence microscopy literature [19, 28–33]. For such classically behaving light, the term “QCRB” is a bit of a misnomer—a consequence of the concept’s origin in quantum parameter estimation [22]. It can be derived in the present context with minimal reference to quantum mechanics [26]. Thus our work is relevant to a broad class of microscopy techniques in which photon correlations are negligible and justifiably ignored.

In step with the growing attention to precise inference of molecular position, microscopists have increasingly adapted the formalisms of statistical parameter estimation [28–34]. In this view, the probability of recording a particular realization of a noisy image \mathbf{I} conditioned on the underlying source position $\mathbf{x} = [x_1, x_2, x_3]^T \equiv$

$[x, y, z]^T$ is $p(\mathbf{I}|\mathbf{x})$. Related to the CRB is the Fisher information (FI) matrix [21], with elements given by:

$$\mathcal{J}_{ij} = \mathbb{E} \left[\left(\partial_{x_i} \log p(\mathbf{I}|\mathbf{x}) \right) \left(\partial_{x_j} \log p(\mathbf{I}|\mathbf{x}) \right) \middle| \mathbf{x} \right], \quad (1)$$

where $\mathbb{E}[\cdot|\mathbf{x}]$ denotes the expectation value conditioned on the value of \mathbf{x} . The counts $I(x_I, y_I)$ recorded at each position (x_I, y_I) are assumed to be independent and distributed according to $I(x_I, y_I)|\mathbf{x} \sim \text{Poisson}(\bar{I}(x_I, y_I; \mathbf{x}))$ for some expected image $\bar{I}(x_I, y_I; \mathbf{x})$ that depends on the microscope’s response function. The same statistics can be obtained from a quantum optical treatment by considering thermal light in the weak-source limit [23–25]. Equation (1) then becomes:

$$\mathcal{J}_{ij} = \iint dA_I \frac{(\partial_{x_i} \bar{I}(x_I, y_I; \mathbf{x})) (\partial_{x_j} \bar{I}(x_I, y_I; \mathbf{x}))}{\bar{I}(x_I, y_I; \mathbf{x})}. \quad (2)$$

We take the convention that $\bar{I}(x_I, y_I; \mathbf{x})$ is normalized; in accordance with our assumptions of statistical independence then the FI for N detected photons is simply $\mathcal{J}^{(N)} = N\mathcal{J}$. The photon-normalized CRB for the parameter x_i is then given by:

$$\sigma_{x_i}^{(\text{CRB})} = \sqrt{[\mathcal{J}^{-1}]_{ii}}, \quad (3)$$

which sets the lower bound for the precision with which any unbiased estimator of x_i can perform [21].

We consider a stochastic field with the following normalized equal-time mutual coherence function [23–27] on the Fourier plane of the microscope:

$$g(x_F, y_F, x'_F, y'_F; \mathbf{x}) = \psi(x_F, y_F; \mathbf{x}) \psi^*(x'_F, y'_F; \mathbf{x}). \quad (4)$$

Here the classical wavefunction in the scalar approximation (in appropriately scaled coordinates) is given by

[35, 36]:

$$\psi(x_F, y_F; \mathbf{x}) = \mathcal{A}(1 - r_F^2)^{-1/4} \text{Circ}\left(\frac{nr_F}{\text{NA}}\right) \times \exp\left[ik\left(xx_F + yy_F + z\sqrt{1 - r_F^2}\right)\right], \quad (5)$$

as illustrated in Fig. 1(a). In Eq. (5) $r_F = \sqrt{x_F^2 + y_F^2}$, n is the index of refraction of the objective immersion medium (assumed matched to that of the sample), NA is the numerical aperture, and the $\text{Circ}(\cdot)$ function restricts support to $r_F < \text{NA}/n$. \mathcal{A} is a normalization factor such that $\iint dA_F |\psi(x_F, y_F)|^2 = 1$, given analytically by:

$$\mathcal{A} = \left[2\pi\left(1 - \sqrt{1 - (\text{NA}/n)^2}\right)\right]^{-1/2}. \quad (6)$$

We assume a quasimonochromatic signal with free-space wavelength λ_o and $k = 2\pi n/\lambda_o$. After the objective we assume paraxial propagation through air and lossless, linear optical elements. We neglect polarization effects, as is appropriate, e.g., for emission from a freely tumbling fluorophore [37]. Note that in Eq. (5), the source position \mathbf{x} affects only the phase at the Fourier plane, based on the assumption that displacements in \mathbf{x} are sufficiently small [36]. Thus recent work on quantum multiphase estimation is relevant [38, 39], though again we stress the classical nature of the problem at hand. In pursuit of the ultimate precision bounds, we here consider the limiting case of zero background light. The expected intensity distribution at the detector is related to $\psi(x_F, y_F)$ via a generic unitary operator U :

$$\bar{I}(x_I, y_I; \mathbf{x}) = \left|U[\psi(x_F, y_F; \mathbf{x})]\right|^2. \quad (7)$$

Thus once U is specified one can compute Eqs. (2) and (3). The form of U depends on the sequence of optical elements (lenses, mirrors, beam splitters, phase elements, etc.) placed between the Fourier plane and the camera. In the simplest case only a tube lens is added [Fig. 1(a)], and the appropriate unitary operation is a scaled Fourier transform $U = \mathcal{F}$ [40]. It is known that this approach produces worse FI for z estimation than for x and y , especially near $z = 0$ [30].

New microscope designs have been developed in recent years with the goal of modifying the PSF in a way that decreases $\sigma_z^{(\text{CRB})}$. A common framework is to modulate the phase at the Fourier plane with some carefully chosen phase mask $\varphi(x_F, y_F)$, e.g., programmed onto a spatial light modulator (SLM) [Fig. 1(b)], such that $U[\psi] = \mathcal{F}[\psi \times \exp(i\varphi)]$ in Eq. (7). This encompasses the astigmatic [9], double-helix [10, 11], and self-bending PSFs [12], among others [13, 14]. Related multifocus techniques [8, 15, 16] can be represented by a series of beam splitters and phase elements. FI has previously been used as a figure of merit for comparison of these techniques [7, 30, 31]. A rational approach to PSF design

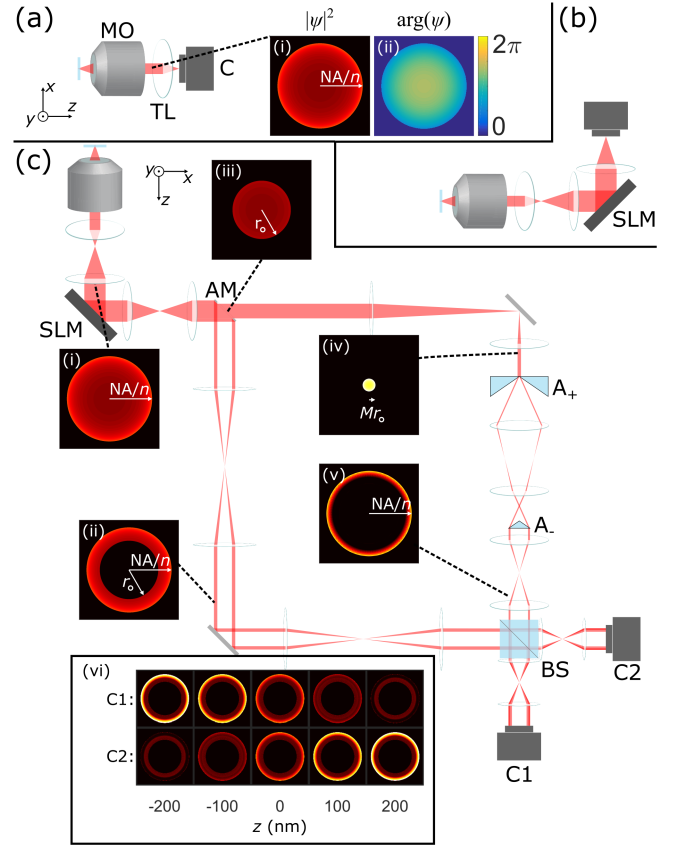


FIG. 1. Single-objective collection schematics. (a) Standard microscope with microscope objective (MO), tube lens (TL) and camera (C). Insets: (i) intensity, (ii) example phase of ψ . (b) Engineered microscope with phase element. Two lenses form a 4f optical correlator [40], within which a phase retarder (e.g. an SLM) is placed. (c) Proposed interferometer for obtaining $\sigma_z^{(\text{QCRB})}$. SLM compensates for defocus accrued downstream. Collected light (i) is split by an annular mirror (AM) with inner radius $r_o = 0.6326$. “Outer” portion (ii) is relayed to the beam splitter (BS) with two unit-magnification telescopes. “Inner” arm (iii) is demagnified with a telescope of magnification $M = 0.22$ (iv), expanded into an annulus with axicon A_+ of phase $\varphi(r_F) = 680 \times r_F$, passed through two relay lenses, recollimated with axicon A_- of phase $\varphi(r_F) = -680 \times r_F$ (v), then relayed to the BS. Intensities illustrated in (i)-(v) have common color scale, except (iv) which has a $5\times$ scale to avoid saturation. Interferometric signals are detected on two cameras C1 and C2 placed at conjugate Fourier planes. Example images recorded on C1 and C2 for various z are shown in (vi). Exact distances between optical elements and diffraction integrals that describe propagation through the apparatus are detailed in [41].

was recently demonstrated by numerically optimizing the mean FI over a specified depth range with respect to a chosen basis for $\varphi(x_F, y_F)$, yielding the saddle-point [31] and tetrapod PSFs [32]. This protocol amounts to specifying a form for U , then maximizing FI w.r.t. a set of parameters on which U depends. Here we seek a more fundamental bound with the form of U unconstrained.

For this we turn to previous work in quantum statistical inference, in which the problem of maximizing FI over all possible positive operator-valued measures has been treated beginning some fifty years ago [22, 42, 43].

To establish the appropriate notation, suppose the photons collected by the microscope are in the state denoted by the density operator $\rho(\mathbf{x})$. We can then define the quantum Fisher information (QFI) \mathcal{K} associated with this state [22, 42–45]:

$$\mathcal{K}_{ij} = \frac{1}{2} \text{Re Tr } \rho (\mathcal{L}_{x_i} \mathcal{L}_{x_j} + \mathcal{L}_{x_j} \mathcal{L}_{x_i}), \quad (8)$$

where \mathcal{L}_{x_i} is the symmetric logarithmic derivative defined implicitly by:

$$\partial_{x_i} \rho = \frac{1}{2} (\mathcal{L}_{x_i} \rho + \rho \mathcal{L}_{x_i}). \quad (9)$$

Analogous to the relation between the CRB and FI, the QCRB is related to the QFI by:

$$\sigma_{x_i}^{(\text{QCRB})} = \sqrt{[\mathcal{K}^{-1}]_{ii}}. \quad (10)$$

The QCRB defined in Eq. (10) bounds the estimation precision for any measurement on the state $\rho(\mathbf{x})$ [22]. For our purposes, we have $\sigma_{x_i}^{(\text{CRB})} \geq \sigma_{x_i}^{(\text{QCRB})}$, regardless of the microscope configuration after the objective lens. Thus we can compare $\sigma_z^{(\text{CRB})}$ associated with state-of-the-art techniques to the ultimate bound set by $\sigma_z^{(\text{QCRB})}$.

To proceed in computing the QFI and QCRB, we specify the single-photon state represented by:

$$\rho(\mathbf{x}) = \iint dA_F \iint dA'_F g(x_F, y_F, x'_F, y'_F; \mathbf{x}) \times |x_F, y_F\rangle \langle x'_F, y'_F| \quad (11)$$

where $|x_F, y_F\rangle = a^\dagger(x_F, y_F)|0\rangle$, and $a^\dagger(x_F, y_F)$ is the creation operator for the specified mode, obeying $[a(x'_F, y'_F), a^\dagger(x_F, y_F)] = \delta(x'_F - x_F)\delta(y'_F - y_F)$. It should be emphasized that the classical optical state we consider in this work is certainly not equivalent to the highly quantum mechanical one-photon state of Eq. (11). Rather it can be shown that under the appropriate approximations (thermal light in the weak-source limit), the optimal value of \mathcal{J} described in Eq. (2) is mathematically equivalent to \mathcal{K} obtained by substitution of Eq. (11) in Eq. (8) [25, 26]. We adopt a similar strategy to that recently used to examine the related problem of resolving two weak thermal point sources [25] (which has since inspired a number of theoretical and experimental follow-up studies [46–57]). The problem of establishing quantum bounds of localizing a single point source has also been considered in a number of contexts over the years [22, 43, 58]. We distinguish our work by deriving expressions for direct comparison to CRBs of existing 3D microscopes, yielding tight bounds and facilitating proof of the (sub)optimality of various advanced techniques.

In the Supplemental Material [41] we derive the QCRBs for 3D localization microscopy using a single microscope objective. The results are:

$$\sigma_x^{(\text{QCRB})} = \sigma_y^{(\text{QCRB})} = C_{xy}/2, \quad (12a)$$

$$\sigma_z^{(\text{QCRB})} = (C_z^{-2} - |\gamma|^2)^{-1/2}/2, \quad (12b)$$

with

$$C_{xy} = \frac{\sqrt{3}}{k\mathcal{A}\sqrt{\pi}} \left[2 - \sqrt{1 - (\text{NA}/n)^2} (2 + (\text{NA}/n)^2) \right]^{-1/2}, \quad (13)$$

$$C_z = \frac{\sqrt{3}}{k\mathcal{A}\sqrt{2\pi}} \left[1 - (1 - (\text{NA}/n)^2)^{3/2} \right]^{-1/2}, \quad (14)$$

and

$$\gamma = ik\mathcal{A}^2\pi(\text{NA}/n)^2. \quad (15)$$

In Fig. 2 we compare the QCRBs to the CRBs pertaining to several choices of microscope configuration, including a standard microscope [Fig. 1(a)] and an astigmatic microscope with $\varphi(x_F, y_F) = \sqrt{6}(x_F^2 - y_F^2)$ (both with $\text{NA} = 1.4$, $n = 1.518$, and $\lambda_o = 670$ nm). Here astigmatic imaging of this strength stands in as a representative for similarly engineered PSFs [Fig. 1(b)], as justified by the facts that this choice obtains the minimum $\sigma_z^{(\text{CRB})}$ near $z = 0$ for any astigmatic strength, and that its local minimum compares favorably to those of other engineered PSFs (Figs. S1 and S2 [41]). Unsurprisingly, the standard microscope obtains the QCRB for lateral localization precision at focus. However, the minima of both the standard and engineered configurations exceed $\sigma_z^{(\text{QCRB})}$ by a factor of approximately 1.5.

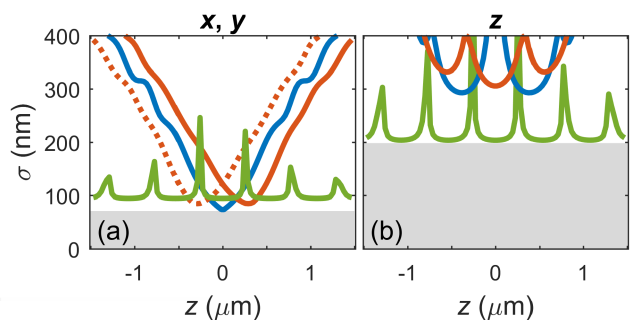


FIG. 2. Photon-normalized QCRBs and measurement CRBs for single-objective collection. For N detected photons divide vertical axis by \sqrt{N} . (a) Lateral localization bounds. Gray shaded region is bounded above by $\sigma = \sigma_x^{(\text{QCRB})} = \sigma_y^{(\text{QCRB})}$. Blue curve: CRB for standard microscope. Red curves (solid is $\sigma_x^{(\text{CRB})}$, dotted is $\sigma_y^{(\text{CRB})}$): astigmatic microscope with strength specified in main text. Green curve: proposed interferometer. (b) Depth localization bounds. Color code corresponds to that in (a).

Computing the QCRB is both straightforward and useful, as it gives crucial context for PSF optimization techniques [31]. Establishing conditions for a measurement that attains the bound is a related topic of interest [38, 39, 45, 59–66]. To show that $\sigma_z^{(\text{QCRB})}$ can indeed be saturated using ordinary optical elements we present the modified Mach-Zehnder apparatus depicted in Fig. 1(c), a variant of a radial shearing interferometer [67]. Exact specifications and the series of diffraction integrals used to compute the CRB for the proposed interferometer are described in detail in [41] (see Fig. S3 and related text). In brief, the collected light is split into two parts using an annular mirror [68]: an inner disk with support $r_F \leq r_o$, and an outer ring with support $r_F \in (r_o, \text{NA}/n)$. In the “outer” arm we (de)magnify the beam by a factor M , then stretch with a pair of axicon prisms [67, 69, 70]. The two portions are recombined with a 50/50 beam splitter and the signal is detected with two cameras placed at conjugate Fourier planes. The parameters r_o and M were optimized over by computing $\sigma_z^{(\text{CRB})}$ for a range of values; Fig. S4 convincingly shows how an increase in r_o results in decreased $\sigma_z^{(\text{CRB})}$ only until the QCRB is saturated [41].

Some calculated images are shown in the inset of Fig. 1(c) for various z . We reiterate that the field is treated classically, e.g., neglecting contributions from field operators of modes in the vacuum state at the input of the beam splitter— a fully quantum mechanical treatment must take these into account [23, 71]. As seen in Fig. 2(b), this interferometer gives $\sigma_z^{(\text{CRB})} \approx 1.03 \times \sigma_z^{(\text{QCRB})}$ near $z = 0$. The prefactor can be made closer to unity by incorporating additional beam splitter stages to make use of the essentially unused inner ring of the “outer” arm. The proposed interferometer approximates projection onto the eigenstates of \mathcal{L}_z (see Fig. S5 and related text in [41]), a condition known to be sufficient for saturating the single-parameter QCRB [45].

Since the signal is recorded in a conjugate Fourier plane and is neither lateral- nor axial-shift-invariant, the proposed interferometer is not a viable configuration for wide-field imaging and is instead more compatible with confocal scanning or feedback-based particle tracking. A perhaps more experimentally attractive variant in which the signal is integrated onto three point detectors rather than two cameras is analyzed in Fig. S6 and gives $\sigma_z^{(\text{CRB})} \approx 1.05 \times \sigma_z^{(\text{QCRB})}$ near $z = 0$ [41]. Practical considerations aside, the main goal of the preceding discussion is to demonstrate that PSF engineering can indeed recover the QCRB even when established configurations evidently fall short. We note that a relative deterioration in lateral precision accompanies the improvement in depth precision for this particular arrangement [Fig. 2(a)], a common occurrence in multiparameter estimation. A measurement that simultaneously saturates the 3D bounds should be possible based on necessary con-

ditions presented in Refs. [38, 64, 72] (see discussion in [41]), the specification of which we reserve for future work.

Advanced fluorescence microscopy implementations sometimes make use of two opposed objectives (Fig. 3) [17–20]. We also consider the quantum bounds for localization using this geometry, for which the state to be plugged into Eqs. (8) and (9) is given by $\rho(\mathbf{x}) = |\psi(\mathbf{x})\rangle \langle \psi(\mathbf{x})|$ now with:

$$|\psi(\mathbf{x})\rangle = \frac{1}{\sqrt{2}} \iint dA_F^{(a)} \psi(x_F^{(a)}, y_F^{(a)}; [x, y, z]^T) \left| x_F^{(a)}, y_F^{(a)} \right\rangle + \frac{1}{\sqrt{2}} \iint dA_F^{(b)} \psi(x_F^{(b)}, y_F^{(b)}; [-x, y, -z]^T) \left| x_F^{(b)}, y_F^{(b)} \right\rangle, \quad (16)$$

where superscripts (a) and (b) refer to the coordinates at the back apertures of objectives a and b (Fig. 3). The results are [41]:

$$\sigma_x^{(\text{QCRB})} = \sigma_y^{(\text{QCRB})} = C_{xy}/2, \quad (17a)$$

$$\sigma_z^{(\text{QCRB})} = C_z/2, \quad (17b)$$

where C_{xy} and C_z are defined as before. Dual-objective QCRBs are depicted in Fig. 4. In an experiment the use of two objectives would double the rate of photon detections, but our normalized expressions scale this effect away. Thus, simply detecting with two cameras without further processing [Fig. 3(a)] leads to the same CRBs as for the standard single-objective microscope (Fig. 4). Another approach is to combine the signals due to objectives a and b interferometrically [Fig. 3(b)] [20]. Interferometric localization microscopy is known to produce superior depth localization precision relative to other common techniques [19]. Interestingly we find that this configuration globally achieves the QCRB in all three dimensions simultaneously. Coinciding saturation of multiparameter bounds is a topic of great current interest in quantum parameter estimation, and dual-objective collection indeed satisfies necessary conditions for the existence of a measurement that saturates the 3D bounds [38, 64, 72] (see [41]). We give further insight in [41], providing analytical expressions that prove optimality for a simplified dual-objective interferometer. That the optimality of this measurement does not depend on the underlying value of \mathbf{x} is another remarkable feature of this finding. These results indicate that no additional optical elements incorporated into the setup in Fig. 3(b) can lead to decreased localization precision bounds, undercutting the naive notion that perhaps combining interferometric and phase engineering techniques can lead to improvement.

In conclusion, by deriving the QCRB for depth localization in a form relevant to advanced single-molecule microscopy techniques, we have proven the (sub)optimality of the CRBs achievable by a number of state-of-the-art

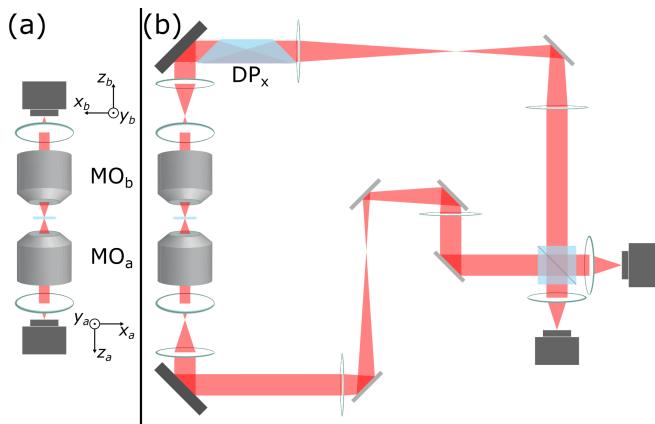


FIG. 3. Dual-objective collection schematics. (a) Signals collected by microscope objectives a and b (MO_a , MO_b) detected on two cameras without recombination. (b) Interferometric detection. Optimal lateral localization requires an additional reflection in one arm, enforced here by an x -oriented Dove prism (DP_x).

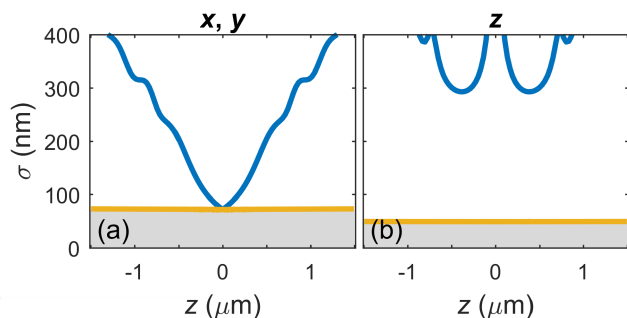


FIG. 4. Photon-normalized QCRBs and measurement CRBs for dual-objective collection. For N detected photons divide vertical axis by \sqrt{N} . (a) Lateral localization bounds. Gray shaded region is bounded above by $\sigma = \sigma_x^{(\text{QCRB})} = \sigma_y^{(\text{QCRB})}$. Blue curve: lateral CRB for non-interferometric detection. Gold line: interferometric detection. (b) Depth localization bounds. Color code corresponds to that in (a).

microscopy configurations. Finite background can be introduced by considering the appropriate mixed photon states, which we reserve for a future study. Our results are relevant for ongoing research on the 3D localization of sources of more complicated photon states, including distinctly nonclassical states. Future work in which the microscope's response function is engineered to increase information about source position (or any other estimandum, e.g., molecular orientation [73]) should be carried out with reference to the measurement-independent bounds.

This material is based upon work supported by, or in part by, the United States Army Research Laboratory and the United States Army Research Office under Grant No. W911NF1510548; as well as the Air Force Office of Scientific Research Grant. No. FA9550-17-1-0371. We

thank Dikla Oren for helpful discussions.

- [1] P. C. Maurer, J. R. Maze, P. L. Stanwix, L. Jiang, A. V. Gorshkov, A. A. Zibrov, B. Harke, J. S. Hodges, A. S. Zibrov, and A. Yacoby, *Nature Physics* **6**, 912 (2010).
- [2] K. Arai, C. Belthangady, H. Zhang, N. Bar-Gill, S. J. Devience, P. Cappellaro, A. Yacoby, and R. L. Walsworth, *Nature Nanotechnology* **10**, 859 (2015).
- [3] J.-C. Jaskula, E. Bauch, S. Arroyo-Camejo, M. D. Lukin, S. W. Hell, A. S. Trifonov, and R. L. Walsworth, *Optics Express* **25**, 11048 (2017).
- [4] H. Zhang, K. Arai, C. Belthangady, J.-C. Jaskula, and R. L. Walsworth, *NPJ Quantum Information* **3**, 31 (2017).
- [5] H. Deschout, F. C. Zanacchi, M. Mlodzianoski, A. Diaspro, J. Bewersdorf, S. T. Hess, and K. Braeckmans, *Nature Methods* **11**, 253 (2014).
- [6] H. Shen, L. J. Tauzin, R. Baiyasi, W. Wang, N. Moringo, B. Shuang, and C. F. Landes, *Chemical Reviews* (2017).
- [7] A. von Diezmann, Y. Shechtman, and W. E. Moerner, *Chemical Reviews* (2017).
- [8] P. Prabhat, S. Ram, E. S. Ward, and R. J. Ober, *IEEE Transactions on Nanobioscience* **3**, 237 (2004).
- [9] B. Huang, W. Wang, M. Bates, and X. Zhuang, *Science* **319**, 810 (2008).
- [10] R. Piestun, Y. Y. Schechner, and J. Shamir, *JOSA A* **17**, 294 (2000).
- [11] S. R. P. Pavani, M. A. Thompson, J. S. Biteen, S. J. Lord, N. Liu, R. J. Twieg, R. Piestun, and W. E. Moerner, *Proceedings of the National Academy of Sciences* **106**, 2995 (2009).
- [12] S. Jia, J. C. Vaughan, and X. Zhuang, *Nature Photonics* **8**, 302 (2014).
- [13] M. D. Lew, S. F. Lee, M. Badieirostami, and W. E. Moerner, *Optics Letters* **36**, 202 (2011).
- [14] D. Baddeley, M. B. Cannell, and C. Soeller, *Nano Research* **4**, 589 (2011).
- [15] M. F. Juette, T. J. Gould, M. D. Lessard, M. J. Mlodzianoski, B. S. Nagpure, B. T. Bennett, S. T. Hess, and J. Bewersdorf, *Nature Methods* **5**, 527 (2008).
- [16] S. Abrahamsson, J. Chen, B. Hajj, S. Stallinga, A. Y. Katsov, J. Wisniewski, G. Mizuguchi, P. Soule, F. Mueller, and C. D. Darzacq, *Nature Methods* **10**, 60 (2013).
- [17] S. W. Hell, S. Lindek, C. Cremer, and E. H. Stelzer, *Optics Letters* **19**, 222 (1994).
- [18] M. G. Gustafsson, D. A. Agard, and J. W. Sedat, *Journal of Microscopy* **195**, 10 (1999).
- [19] C. v. Middendorff, A. Egner, C. Geisler, S. Hell, and A. Schnle, *Optics Express* **16**, 20774 (2008).
- [20] G. Shtengel, J. A. Galbraith, C. G. Galbraith, J. Lippincott-Schwartz, J. M. Gillette, S. Manley, R. Sougrat, C. M. Waterman, P. Kanchanawong, and M. W. Davidson, *Proceedings of the National Academy of Sciences* **106**, 3125 (2009).
- [21] T. M. Cover and J. A. Thomas, *Elements of Information Theory* (John Wiley and Sons, 2012).
- [22] C. W. Helstrom, *Quantum Detection and Estimation Theory* (Academic Press, 1976).
- [23] L. Mandel and E. Wolf, *Optical Coherence and Quantum*

- Optics* (Cambridge University Press, 1995).
- [24] J. W. Goodman, *Statistical Optics* (John Wiley and Sons, 2015).
- [25] M. Tsang, R. Nair, and X.-M. Lu, *Physical Review X* **6**, 031033 (2016).
- [26] M. Tsang, R. Nair, and X.-M. Lu, in *Proc. SPIE*, Vol. 10029 (2016) p. 1002903.
- [27] M. Tsang, *Physical Review A* **97**, 023830 (2018).
- [28] R. J. Ober, S. Ram, and E. S. Ward, *Biophysical Journal* **86**, 1185 (2004).
- [29] S. Ram, E. S. Ward, and R. J. Ober, *Proceedings of the National Academy of Sciences of the United States of America* **103**, 4457 (2006).
- [30] M. Badieirostami, M. D. Lew, M. A. Thompson, and W. E. Moerner, *Applied Physics Letters* **97**, 161103 (2010).
- [31] Y. Shechtman, S. J. Sahl, A. S. Backer, and W. E. Moerner, *Physical Review Letters* **113**, 133902 (2014).
- [32] Y. Shechtman, L. E. Weiss, A. S. Backer, S. J. Sahl, and W. E. Moerner, *Nano Letters* **15**, 4194 (2015).
- [33] J. Chao, E. S. Ward, and R. J. Ober, *JOSA A* **33**, B57 (2016).
- [34] Y. Sun, *Journal of Biomedical Optics* **18**, 111418 (2013).
- [35] P. N. Petrov, Y. Shechtman, and W. E. Moerner, *Optics Express* **25**, 7945 (2017).
- [36] A. S. Backer and W. E. Moerner, *The Journal of Physical Chemistry B* **118**, 8313 (2014).
- [37] M. D. Lew, M. P. Backlund, and W. E. Moerner, *Nano Letters* **13**, 3967 (2013).
- [38] L. Pezze, M. A. Ciampini, N. Spagnolo, P. C. Humphreys, A. Datta, I. A. Walmsley, M. Barbieri, F. Sciarrino, and A. Smerzi, *Physical Review Letters* **119**, 130504 (2017).
- [39] M. A. Ciampini, N. Spagnolo, C. Vitelli, L. Pezz, A. Smerzi, and F. Sciarrino, *Scientific Reports* **6**, 28881 (2016).
- [40] J. W. Goodman, *Introduction to Fourier Optics* (Roberts and Company Publishers, 2005).
- [41] Supplemental Material.
- [42] C. W. Helstrom, *Physics Letters A* **25**, 101 (1967).
- [43] C. W. Helstrom, *JOSA* **60**, 233 (1970).
- [44] A. S. Holevo, *Probabilistic and Statistical Aspects of Quantum Theory*, Vol. 1 (Springer Science and Business Media, 2011).
- [45] S. L. Braunstein and C. M. Caves, *Physical Review Letters* **72**, 3439 (1994).
- [46] J. Rehacek, M. Paur, B. Stoklasa, Z. Hradil, and L. L. Sanchez-Soto, *Optics Letters* **42**, 231 (2017).
- [47] M. Paur, B. Stoklasa, Z. Hradil, L. L. Sanchez-Soto, and J. Rehacek, *Optica* **3**, 1144 (2016).
- [48] Z. S. Tang, K. Durak, and A. Ling, *Optics Express* **24**, 22004 (2016).
- [49] W.-K. Tham, H. Ferretti, and A. M. Steinberg, *Physical Review Letters* **118**, 070801 (2017).
- [50] F. Yang, A. Tashchilina, E. S. Moiseev, C. Simon, and A. I. Lvovsky, *Optica* **3**, 1148 (2016).
- [51] R. Nair and M. Tsang, *Physical Review Letters* **117**, 190801 (2016).
- [52] C. Lupo and S. Pirandola, *Physical Review Letters* **117**, 190802 (2016).
- [53] X.-M. Lu, R. Nair, and M. Tsang, arXiv preprint arXiv:1609.03025 (2016).
- [54] R. Kerviche, S. Guha, and A. Ashok, arXiv preprint arXiv:1701.04913 (2017).
- [55] J. Rehacek, Z. Hradil, B. Stoklasa, M. Paur, J. Grover, A. Krzic, and L. L. Sanchez-Soto, *Physical Review A* **96**, 062107 (2017).
- [56] R. Nair and M. Tsang, *Optics Express* **24**, 3684 (2016).
- [57] S. Z. Ang, R. Nair, and M. Tsang, *Physical Review A* **95**, 063847 (2017).
- [58] M. Tsang, *Optica* **2**, 646 (2015).
- [59] A. Fujiwara and H. Nagaoka, *Physics Letters A* **201**, 119 (1995).
- [60] R. D. Gill and S. Massar, *Physical Review A* **61**, 042312 (2000).
- [61] O. E. Barndorff-Nielsen and R. D. Gill, *Journal of Physics A: Mathematical and General* **33**, 4481 (2000).
- [62] A. Fujiwara, *Journal of Physics A: Mathematical and General* **39**, 12489 (2006).
- [63] A. Luati, *The Annals of Statistics* **32**, 1770 (2004).
- [64] K. Matsumoto, *Journal of Physics A: Mathematical and General* **35**, 3111 (2002).
- [65] P. C. Humphreys, M. Barbieri, A. Datta, and I. A. Walmsley, *Physical Review Letters* **111**, 070403 (2013).
- [66] Y. Chen and H. Yuan, *New Journal of Physics* (2017).
- [67] O. Bryngdahl, *JOSA* **61**, 169 (1971).
- [68] J. Hohlbein and C. G. Hubner, *Applied Physics Letters* **86**, 121104 (2005).
- [69] V. Jarutis, R. Pakauskas, and A. Stabinis, *Optics Communications* **184**, 105 (2000).
- [70] Y. Wang, S. Yan, A. T. Friberg, D. Kuebel, and T. D. Visser, *JOSA A* **34**, 1201 (2017).
- [71] J. H. Shapiro, *IEEE Journal of Selected Topics in Quantum Electronics* **15**, 1547 (2009).
- [72] S. Ragy, M. Jarzyna, and R. Demkowicz-Dobrzanski, *Physical Review A* **94**, 052108 (2016).
- [73] M. P. Backlund, M. D. Lew, A. S. Backer, S. J. Sahl, and W. E. Moerner, *ChemPhysChem* **15**, 587 (2014).